ARTICLE

www.the-innovation.org

Fluctuating magnetic droplets immersed in a sea of quantum spin liquid

Zihao Zhu,[1,11] Binglin Pan,[1,11] Linpeng Nie,[2,11] Jiamin Ni,[1,11] Yanxing Yang,[1] Changsheng Chen,[1] Chengyu Jiang,[1] Yeyu Huang,[1] Erjian Cheng,[1] Yunjie Yu,[1] Jianjian Miao,[3] Adrian D. Hillier,[4] Xianhui Chen,[2,5,6] Tao Wu,[2,5,6,*] Yi Zhou,[7,8,9,*] Shiyan Li,[1,5,10,*] and Lei Shu[1,5,10,*]

*Correspondence: wutao@ustc.edu.cn (T.W.); yizhou@iphy.ac.cn (Y.Z.); shiyan_li@fudan.edu.cn (S.L.); leishu@fudan.edu.cn (L.S.)

Received: February 16, 2023; Accepted: June 8, 2023; Published Online: June 14, 2023; https://doi.org/10.1016/j.xinn.2023.100459

GRAPHICAL ABSTRACT

PUBLIC SUMMARY

- Multiple techniques are used to study QSL candidate $NaYbSe_2$.
- The absence of long-range magnetic order is confirmed by all techniques.
- Coexistence of quasi-static and dynamic spins is observed in both μSR and NMR.
- Results of thermal conductivity suggest the absence of itinerant gapless magnetic excitations.
- A scenario of fluctuating ferrimagnetic droplets immersed in a sea of QSL is proposed.

ARTICLE

Fluctuating magnetic droplets immersed in a sea of quantum spin liquid

Zihao Zhu,[1,11] Binglin Pan,[1,11] Linpeng Nie,[2,11] Jiamin Ni,[1,11] Yanxing Yang,[1] Changsheng Chen,[1] Chengyu Jiang,[1] Yeyu Huang,[1] Erjian Cheng,[1] Yunjie Yu,[1] Jianjian Miao,[3] Adrian D. Hillier,[4] Xianhui Chen,[2,5,6] Tao Wu,[2,5,6,*] Yi Zhou,[7,8,9,*] Shiyan Li,[1,5,10,*] and Lei Shu[1,5,10,*]

[1]State Key Laboratory of Surface Physics, and Department of Physics, Fudan University, Shanghai 200433, China

[2]CAS Key Laboratory of Strongly-coupled Quantum Matter Physics, Department of Physics, University of Science and Technology of China, Hefei, Anhui 230026, China

[3]Department of Physics, the University of Hong Kong, Hong Kong, China

[4]ISIS Pulsed Neutron and Muon Source, STFC Rutherford Appleton Laboratory, Harwell Campus, Didcot, Oxfordshire OX11 0QX, UK

[5]Collaborative Innovation Center of Advanced Microstructures, Nanjing 210093, China

[6]CAS Center for Excellence in Superconducting Electronics (CENSE), Shanghai 200050, China

[7]Institute of Physics and Beijing National Laboratory for Condensed Matter Physics, Chinese Academy of Sciences, Beijing 100190, China

[8]Songshan Lake Materials Laboratory, Dongguan, Guangdong 523808, China

[9]Kavli Institute for Theoretical Sciences and CAS Center for Excellence in Topological Quantum Computation, University of Chinese Academy of Sciences, Beijing 100190, China

[10]Shanghai Research Center for Quantum Sciences, Shanghai 201315, China

[11]These authors contributed equally

*Correspondence: wutao@ustc.edu.cn (T.W.); yizhou@iphy.ac.cn (Y.Z.); shiyan_li@fudan.edu.cn (S.L.); leishu@fudan.edu.cn (L.S.)

Received: February 16, 2023; Accepted: June 8, 2023; Published Online: June 14, 2023; https://doi.org/10.1016/j.xinn.2023.100459

Citation: Zhu Z., Pan B., Nie L., et al., (2023). Fluctuating magnetic droplets immersed in a sea of quantum spin liquid. The Innovation **4(5)**, 100459.

The search of quantum spin liquid (QSL), an exotic magnetic state with strongly fluctuating and highly entangled spins down to zero temperature, is a main theme in current condensed matter physics. However, there is no smoking gun evidence for deconfined spinons in any QSL candidate so far. The disorders and competing exchange interactions may prevent the formation of an ideal QSL state on frustrated spin lattices. Here we report comprehensive and systematic measurements of the magnetic susceptibility, ultralow-temperature specific heat, muon spin relaxation (μSR), nuclear magnetic resonance (NMR), and thermal conductivity for $NaYbSe_2$ single crystals, in which Yb^{3+} ions with effective spin-1/2 form a perfect triangular lattice. All these complementary techniques find no evidence of long-range magnetic order down to their respective base temperatures. Instead, specific heat, μSR, and NMR measurements suggest the coexistence of quasi-static and dynamic spins in $NaYbSe_2$. The scattering from these quasi-static spins may cause the absence of magnetic thermal conductivity. Thus, we propose a scenario of fluctuating ferrimagnetic droplets immersed in a sea of QSL. This may be quite common on the way pursuing an ideal QSL, and provides a brand new platform to study how a QSL state survives impurities and coexists with other magnetically ordered states.

INTRODUCTION

Quantum spin liquid (QSL) is a highly entangled quantum state in which spins remain disordered and dynamic even down to absolute zero temperature because of strong quantum fluctuations.[1–6] Such an exotic state was first proposed from the study of the triangular-lattice Heisenberg antiferromagnets in 1973 by Anderson.[1] Since QSL has potentially tight relationship with high-temperature superconductivity[7] and quantum information applications,[8] it has gained continuous attention in condensed matter physics. The QSL states are characterized by fractional spin excitations, such as spinons, and the detection of these excitations is a crucial issue for identifying QSL in real materials.[2–6] Several QSL candidates have been suggested by experiments, typical examples include triangular-lattice organic compounds κ-$(BEDT\text{-}TTF)_2Cu_2(CN)_3$[9–11] and $EtMe_3Sb[Pd(dmit)_2]_2$,[12–14] kagome-lattice $ZnCu_3(OH)_6Cl_2$,[15–19] honeycomb lattice α-$RuCl_3$,[20–23] and $H_3LiIr_2O_6$.[24] Despite numerous efforts made in both theoretical and experimental sides, finding realistic smoking gun evidence for QSLs remains the most challenging task in this field. One of the obstacles comes from the ambiguous role played by the impurities and competing exchange interactions: are they fatal or vital to the survival of a QSL?

In recent few years, the inorganic compound $YbMgGaO_4$, in which Yb^{3+} ions with effective spin-1/2 form a perfect triangular lattice, was argued to have a QSL ground state.[25–27] Although muon spin relaxation (μSR) experiments are consistent with persistent spin dynamics and no static magnetism ≥ 0.003 μ_B per Yb ion,[28,29] the absence of magnetic thermal conductivity at extremely low temperature casts doubts,[30] and the observation of frequency-dependent peak of AC magnetic susceptibility suggests a spin-glass ground state in $YbMgGaO_4$.[31] It was argued that the random occupation between Mg^{2+} and Ga^{3+} can induce distortions and result in a disorder of magnetism that mimics the QSL state.[32] Thus, a random spin singlet state, or valence bond glass, was proposed to account for the observations.[33–35]

Compared with $YbMgGaO_4$, the family of Yb dichalcogenide delafossites $NaYb(O, S, Se)_2$ with effective spin-1/2 has a simpler structure, thus is free from the Mg-Ga disorders in non-magnetic layers.[36,37] As shown in Figure 1A, in the structure of $NaYbSe_2$, magnetic Yb^{3+} ions form flat triangular layers, and each Yb^{3+} ion has 6-fold coordination with Se atoms to form a $YbSe_6$ octahedron. Interlinked between these flat triangular layers are sheets of Na atoms, which was once believed to be a perfect frustration system to clarify whether there is a QSL ground state in clean triangular lattice of Yb^{3+} ions. However, it was reported that approximately 5% Na sites are occupied by Yb in $NaYbSe_2$ single crystal.[38]

All three compounds $NaYb(O, S, Se)_2$ are free from long-range order (LRO) down to 50 mK determined from zero field (ZF) specific heat and μSR measurements.[36–41] However, including an isostructural compound $CsYbSe_2$, all of them have field-induced magnetic orders.[39,42–45] Very recently, the ground state of $NaYbSe_2$ is claimed to be a QSL with spinon Fermi surface.[38] A similar result is also reported in $NaYbS_2$.[46] Pressure-induced superconductivity is also observed in $NaYbSe_2$,[47,48] opening up a promising way to study the mechanism of superconductivity in QSL candidates.

Here we report the magnetic susceptibility, specific heat, μSR, nuclear magnetic resonance (NMR), and ultralow-temperature thermal conductivity measurements on $NaYbSe_2$ single crystals. The absence of magnetic order and spin glass is confirmed by different techniques down to 50 mK. With decreasing temperature in ZF, a hump followed by a linear temperature-dependent specific heat is observed. In μSR and NMR measurements, both quasi-static and dynamic spins are found clearly in $NaYbSe_2$. Furthermore, the residual linear term of thermal conductivity at all fields is negligible, pointing to the absence of itinerant fermionic magnetic excitations in $NaYbSe_2$. Our data reveal that $NaYbSe_2$ hosts a ground state of fluctuating ferrimagnetic droplets immersed in a sea of QSL on Yb^{3+} triangular lattice.

RESULTS

The temperature dependences of magnetic susceptibility χ of $NaYbSe_2$ in external magnetic field $\mu_0 H = 1$ T in two different directions are plotted in Figure 1B. The absence of magnetic phase transition is confirmed down to 2 K. There is no splitting between ZF cooling and field cooling curves of magnetic susceptibility (Figure S2A), suggesting no spin glass in the system down to 2 K. The inset of Figure 1B presents a Curie-Weiss (CW) fit with field perpendicular to the c axis. The data above 100 K can be well fitted by CW law, giving effective moment $\mu_{eff} = 4.54$ μ_B and the CW temperature $\Theta_{CW} = -49.0$ K. The value of μ_{eff} agrees with the theoretical prediction 4.54 μ_B for trivalent Yb^{3+} ion with $J = 7/2$. Similar to $YbMgGaO_4$,[25,27] magnetization M remains unsaturated but is smaller up to 7 T at 2 K in $NaYbSe_2$ (Figure S2B). The larger absolute value of the CW temperature and smaller M indicate stronger anti-ferromagnetic (AFM) interactions in $NaYbSe_2$.

The temperature dependence of specific heat of $NaYbSe_2$ in various fields ($H \parallel c$) from 0.05 to 20 K are shown in Figure 1C. Consistent with magnetic

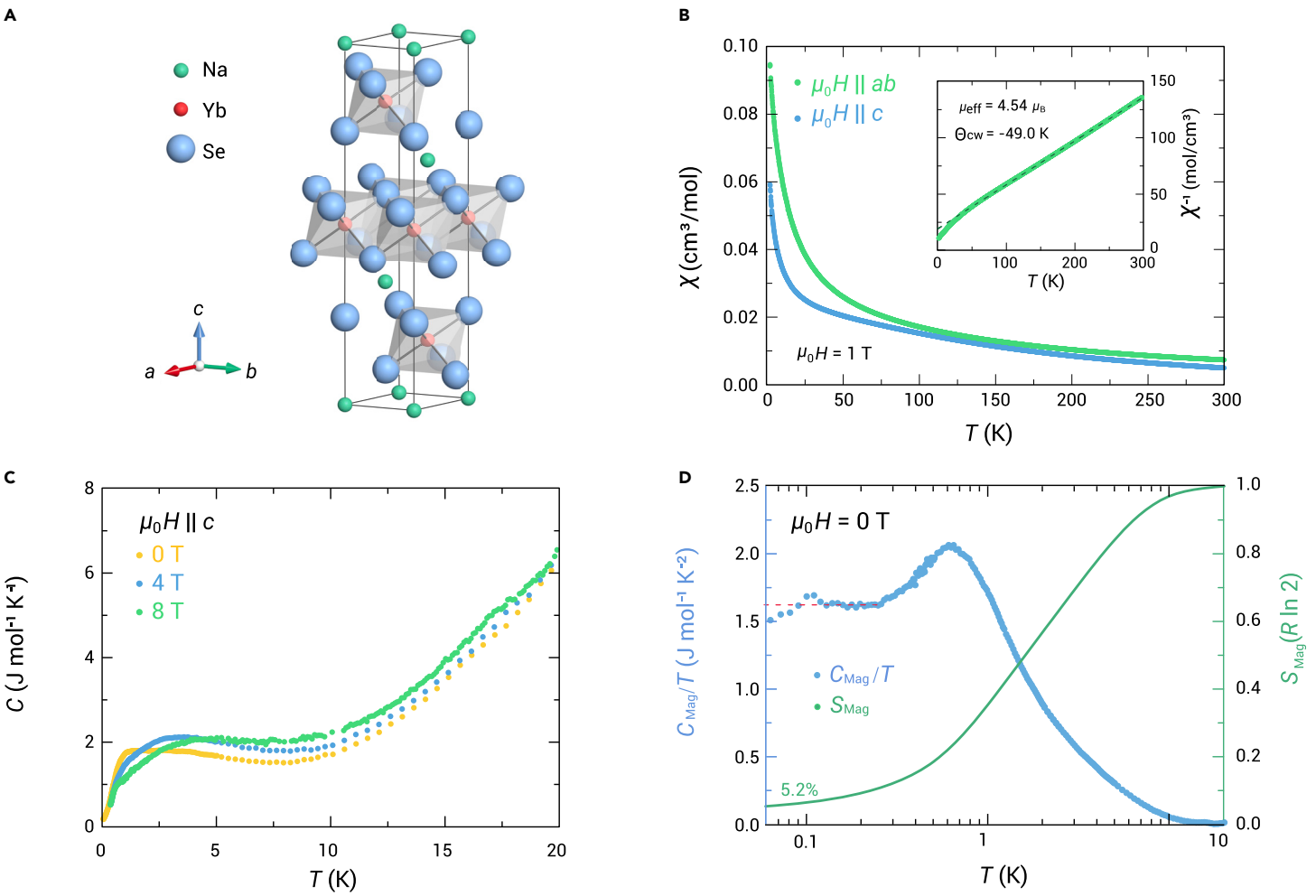

Figure 1. Basic properties of $NaYbSe_2$ (A) The unit cell of $NaYbSe_2$. Green spheres, Na; red spheres, Yb; blue spheres, Se. (B) The temperature dependence of magnetic susceptibility at μ_0H = 1 T of $NaYbSe_2$. The inset shows the fitting result of CW law at T > 100 K. (C) The temperature dependence of specific heat C at μ_0H = 0, 4, and 8 T. (D) The magnetic specific heat C_{Mag}/T and the calculated magnetic entropy S_{Mag} at ZF. The red dashed line is a guide to eyes to show that C_{Mag}/T is temperature independent at low temperature.

susceptibility and former reports,[38,44] no sharp anomaly of LRO is observed in $NaYbSe_2$ in ZF. With decreasing temperature, a broad hump of specific heat shows up, whose position shifts to a higher temperature in magnetic field. However, we do not observe the field-induced transition peak reported previously, because of the lack of the sufficiently strong field.[44] For the ZF data, after subtracting the contributions from phonon and nuclear Schottky anomaly (Figure S3), we obtain the magnetic contribution of specific heat C_{Mag}/T as shown in Figure 1D. We should emphasize that the broad hump is not caused by a crystal electric field (CEF) effect, since the energy gap of CEF is approximately 15 meV, which should appear above 100 K.[38,49] As guided by the red dashed line, the temperature-independent behavior of C_{Mag}/T below 0.25 K is consistent with a spinon Fermi surface.[38] By integrating C_{Mag}/T, we obtain the magnetic entropy S_{Mag}, as shown in Figure 1D. For an effective spin-1/2 system, the theoretical magnetic entropy is R ln 2, where R is the gas constant. The residual entropy of $NaYbSe_2$ at 50 mK is only 5.2% of total entropy. Such little entropy remaining suggests low-temperature physics is dominated by quantum fluctuations rather than thermal fluctuations, indicating the existence of QSL.

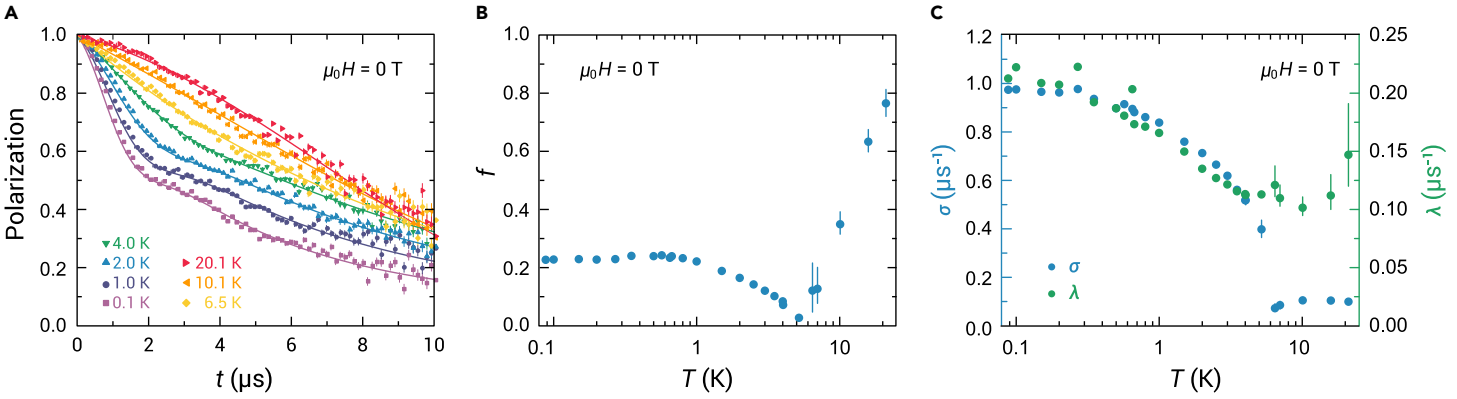

Figure 2. ZF μSR experiment (A) Time spectra of ZF-μSR at representative temperatures. The curves are the fittings using Equation 1. (B) Temperature dependence of fraction of quasi-static spins. (C) Temperature dependence of relaxation rate caused by quasi-static and dynamic spins σ (blue spheres) and λ (green spheres), respectively. The error bars are statistical standard deviation in A, and are determined by the least square method in (B and C).

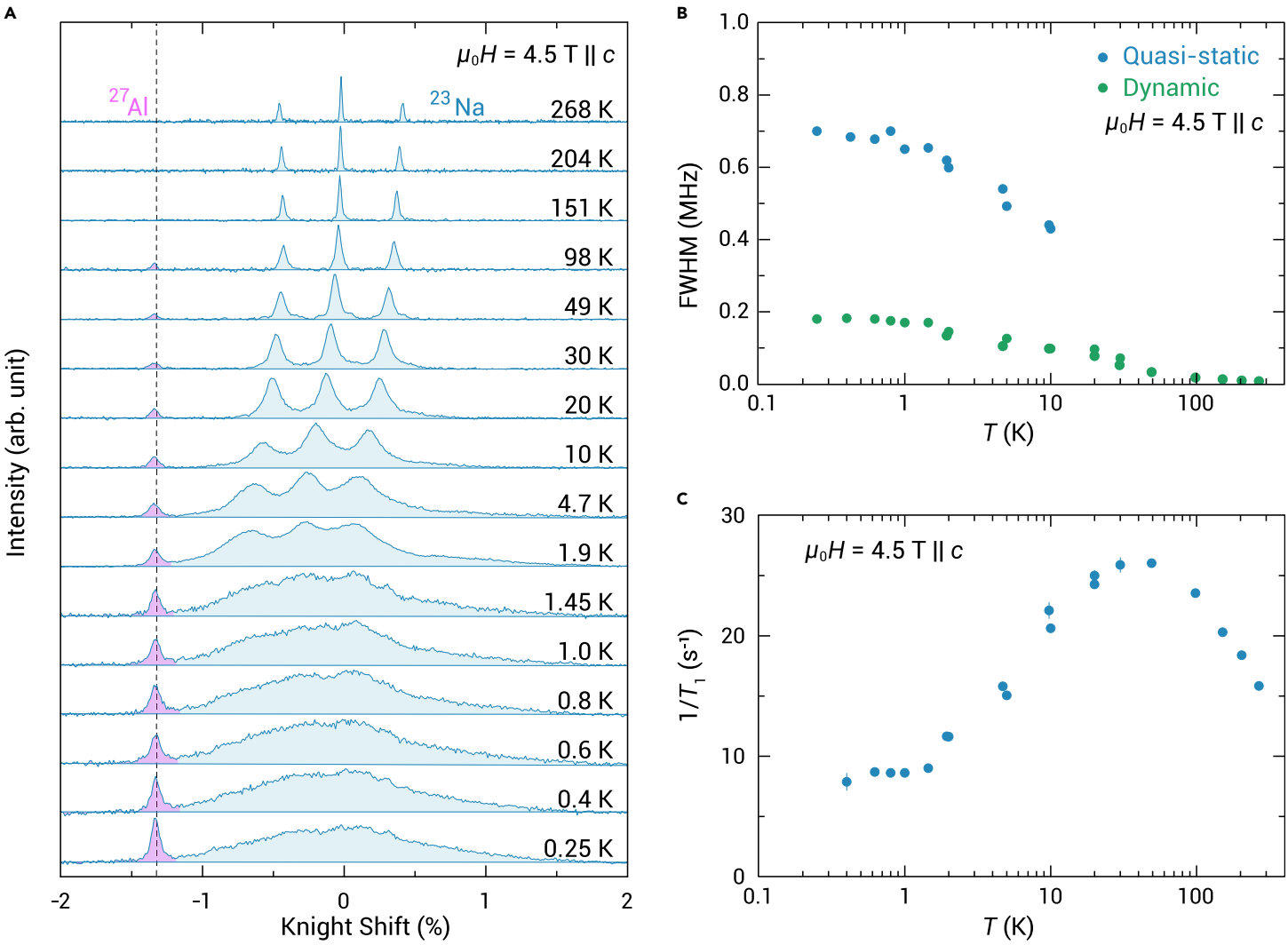

Figure 3. ^{23}Na NMR experiments at 4.5 T (A) NMR spectra of ^{23}Na nuclei with external field μ_0H = 4.5 T parallel to *c*-axis. The sharp magenta peak guided by the black dashed line is the ^{27}Al peak, which is used to calibrate the magnetic field. (B) The temperature dependence of NMR linewidth derived from the spectra as described in SM. The quasi-static (blue spheres) and dynamic (green spheres) components can be easily separated. (C) The temperature dependence of the spin-lattice relaxation rate $1/T_1$. The error bars are determined by the least square method in (B and C).

Both μSR and NMR, which measure spin dynamics at different frequency ranges, are powerful tools in clarifying the static and/or dynamic nature of the magnetic ground state. μSR, which uses muon as a probe, is more sensitive to local magnetic field.[28,50–53] As shown in Figure 2A, the time spectra of muon polarization $P(t)$ in ZF clearly indicates that LRO, which usually induces oscillations in the spectra, is absent in ZF-μSR down to 88 mK. Similar time spectra of muon polarization $P(t)$ has been obtained previously[54]; however, we find that the relaxation process of ZF-μSR can be best described by the sum of a Kubo-Toyabe (KT) term and an exponential term:

$$P(t) = fG_{KT}(\sigma, t) + (1 - f)\exp(-\lambda t), \qquad \text{(Equation 1)}$$

where f is the fraction of the KT term. The fitting function is exactly the same as the $NaYbS_2$ case.[41] The KT term originates from an isotropic Gaussian distribution of randomly oriented static or quasi-static local fields, whose relaxation rate σ is proportional to the root-mean-square width of the distribution.[50] The exponential term with relaxation rate λ originates from dynamic spins. The successful fitting with the above function strongly suggests the coexistence of distinguishable quasi-static spins and dynamic spins.

The temperature dependence of f, σ, and λ are plotted in Figures 2B and 2C. At high temperatures, the value of f is equal to 1, indicating a trivial paramagnetic state, which is also supported by a temperature-independent NMR intensity (see Figure S7B and related discussion in Supplementary Materials). Because of the magnetic exchange interaction, with decreasing temperature from 20 K to 6 K, the system gradually turns into a non-trivial paramagnetic state, in which spin correlation is established and significant spin dynamic appears. As a result, f decreases continuously and the second term in Equation 1 appears. Below 6 K, the temperature-dependent f stops decreasing and upturns, while the temperature-dependent σ also increases clearly below 6 K. These results strongly suggest the formation of quasi-static spins at low temperatures. However, both σ and f saturates to a finite value at low temperatures, and the saturation value of f indicates that only 23% of the sample becomes quasi-static at base temperature. In contrast, the temperature-dependent λ also increases below 4 K, supporting the enhancement of spin dynamics at low temperatures. The temperature-independent behavior of λ below 0.2 K suggests the existence of persistent spin dynamics. We would like to emphasize that these fitting parameters are fully independent and reproducible (see Figure S4 and S5 and related discussion in supplemental information.) Additional evidence for the coexistence of quasi-static and dynamic spins in $NaYbSe_2$ comes from a longitudinal field (LF) μSR, which yields that the fluctuation rate ν at 0.1 K is 2.8 MHz (Figure S4), larger than 1.7 MHz in $NaYbS_2$.[41]

Similar evidence for the coexistence of quasi-static and dynamic spins is also found in ^{23}Na NMR experiments. As shown in Figure 3A, the three-peak structure of ^{23}Na NMR spectra at high temperature comes from quadrupole splitting of nuclei with spin number I = 3/2 (Figure 3A). With temperature decreasing, a tiny asymmetry in spectrum appears below 49 K, suggesting a new component also with three-peak structure (Figures S6A and S9), which is ascribed to the quasi-static spins as observed by our ZF-μSR measurement. As shown in

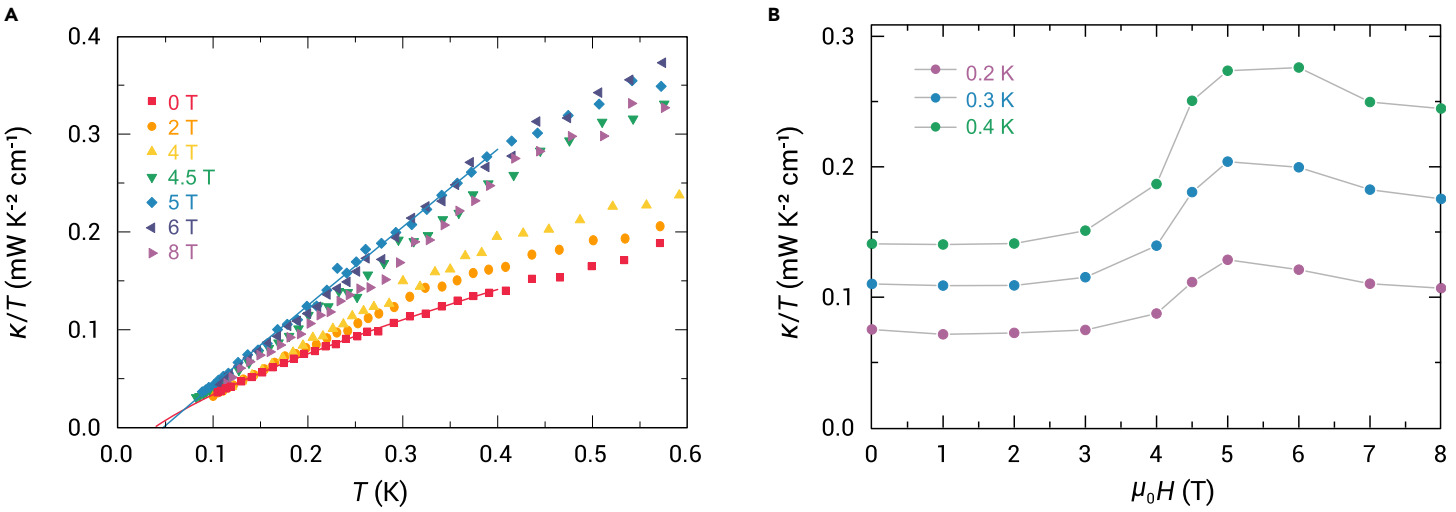

Figure 4. In-plane thermal conductivity (A) The in-plane thermal conductivity of $NaYbSe_2$ in various fields ($\mu_0 H \parallel c$). The solid lines are the fits to the data of 0 and 5 T below 0.4 K using Equation 2. (B) The field dependence of κ/T at 0.2, 0.3, and 0.4 K, respectively.

Figure 3B, the temperature dependence of full width at half-maximum shows a similar increasing behavior for these two components below 49 K, which indicates a close correlation between these two components beyond simple competition. Generally, the demagnetization effect on internal magnetic field should be taken into account for linewidth broadening. However, since the sample used in the present NMR measurements has a shape of thin flake, the demagnetization effect can be neglected in the following analysis (see details in the discussion of Figure S8). The quasi-static moment can be estimated from the broad part of NMR spectra, yielding a small value of 0.13 μ_B (Figure S7). This result indicates that the quasi-static spins in $NaYbSe_2$ are still fluctuating, which is in sharp contrast with traditional spin glass.[55,56] It should be noted that, although a similar spectral broadening at a higher magnetic field, which was ascribed to a field-induced magnetic ordering, has been observed in previous NMR work on $NaYbSe_2$[44] and $NaYbO_2$,[42] the lower magnetic field used in the present work only leads to the formation of magnetic droplets instead of a uniform magnetic ordering. This is also supported by the absence of a peak-like behavior in the temperature-dependent nuclear spin-lattice relaxation rate $1/T_1$.

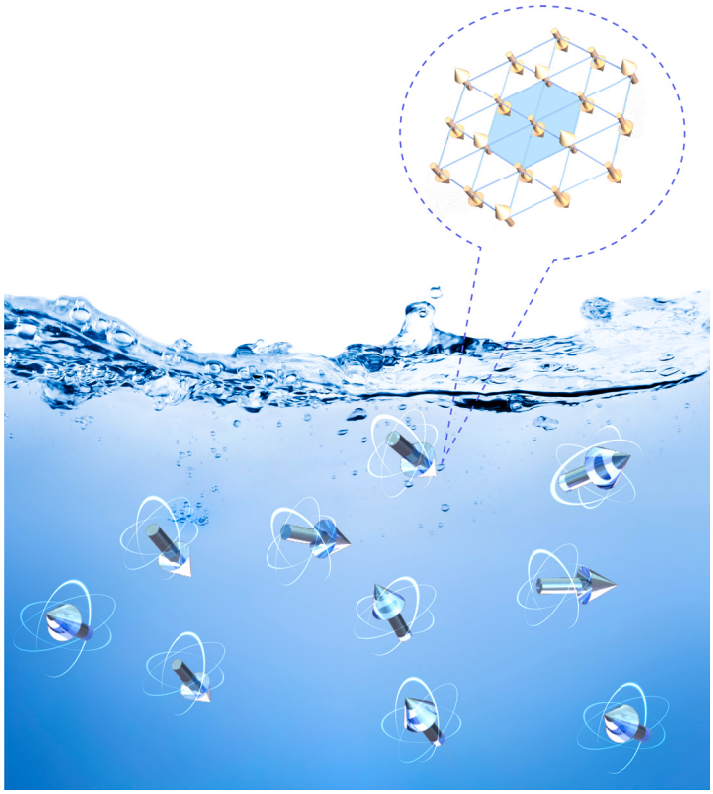

Figure 5. Magnetic droplets immersed in a sea of QSL Each droplet has an up-up-down and $\boldsymbol{Q} = (1/3, 1/3)$ ferrimagnetic structure.

Beside the NMR spectrum, the nuclear spin-lattice relaxation also supports the coexistence of quasi-static and dynamic spins. Inhomogeneous spin dynamics are indeed observed below 2 K accompanied by the above two-component behavior in spectrum. As shown in Figure S6C, the stretching exponent β, which usually depicts the inhomogeneity of spin dynamics, decreases clearly below 2 K with the value well below 1. Especially at the lowest temperature of 0.25 K, there is a clear two-component behavior appearing in the recovery curve of T_1 process (Figure S6B), which is beyond a single T_1 fitting with stretching exponent. This is in line with the scenario proposed above with the coexistence of quasi-static and dynamic spins. Finally, the temperature dependence of the spin-lattice relaxation rate $1/T_1$ extracted from the stretched exponential fitting is plotted in Figure 3C. The broad hump feature around 50 K is usually ascribed to the development of strong spin correlation at a low temperature or CEF effect.[42] The absence of magnetic order is confirmed again by the absence of any significant critical fluctuation at low temperatures. Below 2 K, $1/T_1$ saturates to a constant, coinciding with the persistent spin dynamics observed in μSR experiments. This result also excludes the possibility of a trivial spin glass phase, suggesting a novel magnetic ground state in $NaYbSe_2$.

To further check the existence of gapless magnetic excitations, we performed thermal conductivity measurements to probe the possible itinerant excitations. As for a QSL candidate, thermal conductivity measurement is highly advantageous in probing such elementary excitations, since it is only sensitive to itinerant excitations. In a solid, the contributions to thermal conductivity come from various quasi-particles, such as phonons, electrons, magnons, and spinons. Since $NaYbSe_2$ is an insulator, electrons do not contribute to the thermal conductivity at ultralow temperatures. Additionally, the contribution of magnons can be ruled out because of the absence of magnetic order down to 50 mK. Therefore, thermal conductivity κ at ultralow temperatures can be described by the formula

$$\kappa = aT + bT^{\alpha}, \qquad \text{(Equation 2)}$$

where aT and bT^{α} represent the contribution from possible itinerant gapless fermionic magnetic excitations and phonons, respectively.[57,58] Because of the specular reflections of phonons at the sample surfaces, the power α in the second term is typically between 2 and 3.[57,58]

The in-plane thermal conductivity of $NaYbSe_2$ in zero and various fields ($\mu_0 H \parallel c$) are shown in Figure 4. In ZF, the fitting to the data below 0.4 K gives the residual linear term $\kappa_0/T \equiv a = -0.038 \pm 0.007$ mW K^{-2} cm^{-1} and $\alpha = 1.66 \pm 0.04$. This unusual behavior is very similar to $YbMgGaO_4$,[30] both in the unphysical negative κ_0/T and abnormally low value of α ($\kappa_0/T = -0.025 \pm 0.002$ mW K^{-2} cm^{-1} and $\alpha = 1.85 \pm 0.04$ for $YbMgGaO_4$).[30] For comparison, we also measured the thermal conductivity of the non-

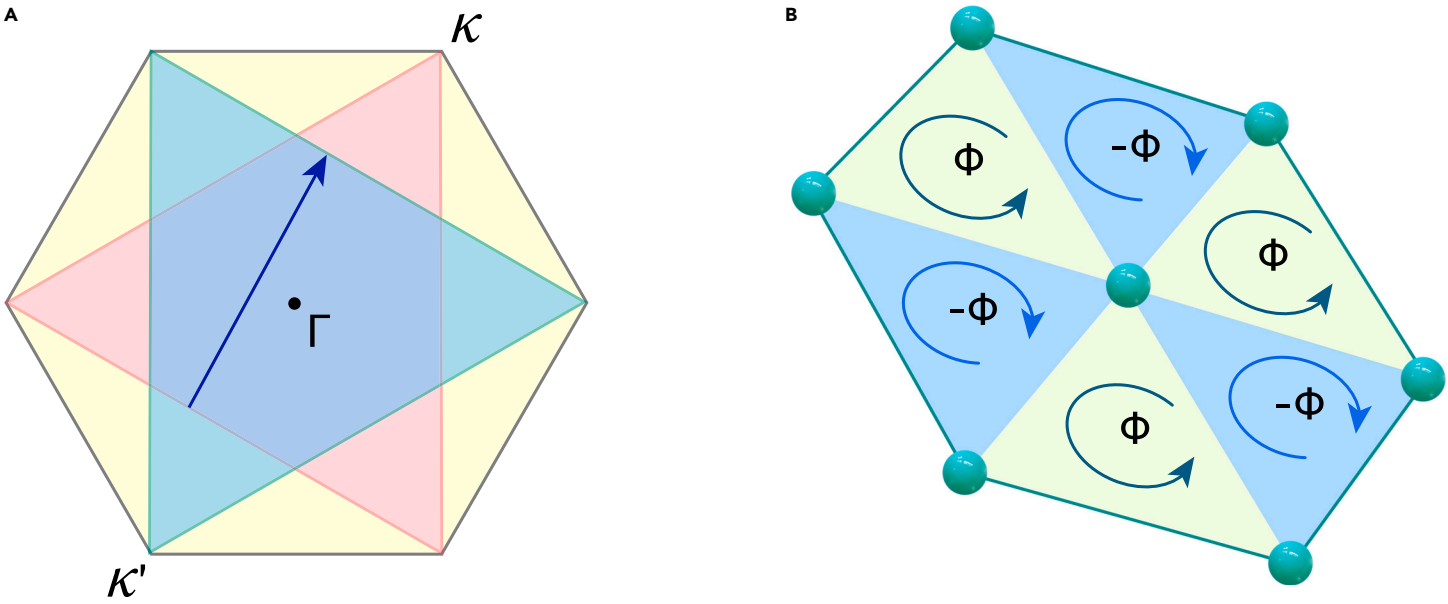

Figure 6. Spinon Fermi surfaces and gauge fluxes in the theoretical model (A) Spinon Fermi surfaces. Black hexagon denotes the first Brillouin zone. Red and blue triangles are Fermi surfaces for spin up and down spinons, respectively, where the flux is chosen to be $\Phi = \pi/2$. The arrow indicates the nesting wave vector $\boldsymbol{Q} = (1/3, 1/3)$. (B) Staggered gauge fluxes.

magnetic $NaLuSe_2$ single crystal, as plotted in Figure S10. There is no magnetic field effect on the thermal conductivity of $NaLuSe_2$, and its thermal conductivity shows a typical phonon behavior in the boundary scattering limit, with $\kappa_0/T = -0.008 \pm 0.010$ mW K^{-2} cm^{-1} and $\alpha = 2.57 \pm 0.05$. More important, the magnitude of thermal conductivity for $NaYbSe_2$ is lower than that of $NaLuSe_2$. Again, this is a similar situation to $YbMgGaO_4$, which has a lower magnitude than non-magnetic $LuMgGaO_4$.[30] We note that the magnitude of κ/T is comparable between $NaYbSe_2$ and $YbMgGaO_4$ in ZF. Previously, we estimated the upper limit of the spinon (if it exists) means a free path in $YbMgGaO_4$ is 8.6 Å, approximately 2.5 times that of the interspin distance.[30] Considering the comparable κ/T and similar triangular Yb lattice, the spinon mean free path in $NaYbSe_2$ should also be no more than 10 Å. In Figure 4A, the fitting to the data of $\mu_0 H = 5$ T gives $\kappa_0/T = -0.041 \pm 0.001$ mW K^{-2} cm^{-1} and $\alpha = 1.97 \pm 0.05$. Therefore, κ_0/T is virtually zero in all fields, indicating the absence of itinerant gapless magnetic excitations in $NaYbSe_2$, and its thermal conductivity is mainly contributed by phonons. Figure 4B plots the field dependence of the κ/T at 0.2, 0.3, and 0.4 K. For $\mu_0 H < 3$ T, κ/T is independent of fields. With increasing fields, the spins are increasingly polarized, thus reducing the scattering of phonon, leading to the rapid enhancement of thermal conductivity from 3 to 5 T, as observed in $YbMgGaO_4$.[30]

DISCUSSION

We now turn to discuss the ground state of $NaYbSe_2$. The absence of LRO and spin glass in $NaYbSe_2$ is confirmed down to 50 mK. Both μSR and NMR experiments point out that a minority of quasi-static spins and a majority of dynamic spins co-exist in $NaYbSe_2$ down to the base temperature. In fact, our specific heat measurements also hint at this picture. The broad hump of C_{Mag}/T at approximately 0.8 K comes from the correlations of quasi-static spins, while the temperature-independent behavior below 0.25 K suggests the existence of well-defined magnetic excitations, which is an essential feature of gapless QSLs.[24,38,39] Comparing our results in ZF, these two characteristic temperatures coincide with our μSR data astonishingly. We note that the external field applied in the NMR experiments could affect the ground state, and the experimental principles of NMR and μSR are different, so the results of NMR cannot be compared with μSR or specific heat directly. As for the thermal conductivity measurements, the dynamic spins should result in a finite residual linear term κ_0/T in $NaYbSe_2$.[59–61] However, the gapless spinons may be strongly scattered by the quasi-static spins, leading to a negligible κ_0/T.

We propose here a possible picture of a mixed state of fluctuating short-range up-up-down ferrimagnetic droplets and QSL. As for the minority quasi-static spins, there are no long-range but at least short-range correlations between them. Since there is AFM interaction on a triangular lattice, the total moment cannot be canceled. Therefore, we take the state as an up-up-down ferrimagnetic state. They are not static like spin glass, and our NMR result suggests that they are still fluctuating. They only take 23% of the total spins, suggesting they distribute in the system like droplets. Such droplets might come from the 5% wrong occupation at Na sites, which is difficult to avoid.[38] Note that such 5% site-mixing (Na-Yb) ratio is obtained by single-crystal X-ray refinements, while the powder neutron scattering refinement suggests an upper limit of 10% of Yb at the Na site.[38] From our powder X-ray refinements (data not shown), this ratio is approximately 11.6%. When it comes to the dynamic spins, they remain disordered and fluctuating down to our base temperature, exactly matching the definition of QSL. The evidence for spinon Fermi surface was also given by our specific heat measurements. Additionally, there is only < 5.2% residual entropy at zero temperature, also indicating the presence of QSL. The same scenario was also proposed for $NaYbS_2$.[41]

Now it brings us to why other methods like magnetic susceptibility and neutron scattering do not observe such ferrimagnetic droplets.[36,38] For the magnetic susceptibility technique, it is more sensitive to slower fluctuations, whose limit is about 10^4 Hz, while NMR and μSR are more sensitive to faster fluctuations. Hence a state could be dynamic in magnetic susceptibility measurements, but quasi-static in NMR and μSR. In inelastic neutron scattering experiments, such fluctuating droplets could also mimic spinon continuum because of its randomness, making it difficult to differentiate.

The ferrimagnetic droplets immersed in a sea of QSL are illustrated in Figure 5, on which an up-up-down magnetic structure forms within each droplet in accordance with field-induced AFM orders in Yb^{3+} compounds on triangular lattice.[39,42–45] It is natural to assume that such a ferrimagnetic ordering state has a slightly higher energy than the QSL state, which allows the nucleation of ferrimagnetic droplet around a defect. Meanwhile, the thermal fluctuation of these magnetic droplets will give rise to the residual entropy. The ratio between the residual entropy and the total magnetic entropy is estimated to be $\frac{r\ln(1+m/3)}{m\ln 2}$, where r is the volume fraction of droplets and each droplet carries m Yb^{3+} ions. It is expected that the size of the fluctuating droplets will be enhanced by an external magnetic field, resulting in a long-ranged AFM order in bulk when the applied magnetic field exceeds some threshold.[39,42–45]

Other remaining issues include why an impurity favors a $\boldsymbol{Q} = (1/3, 1/3)$ magnetic droplet in such a QSL and what kind of QSLs can host this possibility. These issues can be addressed by assuming a nested (or nearly nested) spinon Fermi surface as illustrated in Figure 6A, which indicates the instability of the spinon Fermi surface. Thus, a spinon density wave, that is, a magnetic ordered structure of the wave vector $\boldsymbol{Q} = (1/3, 1/3)$ will be energetically favored. An impurity in a

QSL background can be viewed as a hole of local magnetic moments. It will generate a Ruderman-Kittel-Kasuya-Yosida-like (RKKY) oscillation that is characterized by the spin susceptibility function $\chi(\boldsymbol{q},\omega=0)$, provided that there exists a spinon Fermi surface. If the spinon Fermi surface becomes nested, the spin susceptibility $\chi(\boldsymbol{q},\omega=0)$ will diverge at the nesting wave vector $\boldsymbol{q}=\boldsymbol{Q}$, resulting in a magnetic ordering in short range, so that the nucleation of a $\boldsymbol{Q}=(1/3,1/3)$ magnetic droplet comes into being around the impurity.

However, an usual spin rotationally invariant system, such a nested Fermi surface, leads to a 1/3-filling spinon band instead of the 1/2-filling spinon band (see Figure 6A) required by the Mottness. This seeming contradiction can be resolved by considering the spin-orbit interaction that comes from the buckling of Se atoms and spoils the spin rotational symmetry. Because of the buckling, triangular layers $YbSe_6$ has a $D_{3d}=D_3\times I=C_{3v}\times I$, but not C_6 rotational symmetry. To solve the problem, we consider an effective Hamiltonian as follows,

$$H_{\text{eff}}=-t\sum_{\langle mn\rangle,s}e^{is\theta_{mn}}c^{\dagger}_{ms}c_{ns}, \qquad \text{(Equation 3)}$$

where $\langle mn\rangle$ denotes a pair of nearest neighbor sites m and n on a triangular lattice, $c^{\dagger}_{ms}$ creates a fermionic spinon, $s=\pm1$ refers to up (down) spin (or to be precise, pseudospin), and θ_{mn} are phases that give rise to staggered gauge fluxes $\pm\Phi$ on elementary triangles (see Figure 6B). Note that both C_{3v} and the time-reversal symmetry are respected by the Hamiltonian H_{eff}, because the net gauge flux through a unit cell (containing two triangles) is zero. However, the spatial inversion symmetry I is been broken. When $\Phi=0$, the spin-rotational symmetry is restored, together with the spatial inversion symmetry, yielding in a circle spinon Fermi surface at 1/2-filling. When $\Phi\neq0$, up and down spinons possess two different Fermi surfaces at 1/2-filling. These two Fermi surfaces can be transformed to each other under a time-reversal or a reflection. In particular, when $\Phi=\pi/2$ (or $-\pi/2$), as illustrated in Figure 6A, the two spinon Fermi surfaces become two perfect triangles, and their edges are nested by a wave vector $\boldsymbol{Q}=(1/3,1/3)$ or its C_3 rotations. Therefore, we suggest that the QSL depicted by the effective Hamiltonian H_{eff} in Equation 3 is a promising candidate for the paramagnetic phase bordering a $\boldsymbol{Q}=(1/3,1/3)$ magnetic ordering state in $NaYbSe_2$. The QSL to magnetic ordering phase transition occurs at $\Phi=\pm\pi/2$.

CONCLUSION

We present specific heat, μSR, NMR, and thermal conductivity measurements on triangular-lattice compound $NaYbSe_2$ single crystals to figure out its ground state. The absence of long-range magnetic order and spin glass is confirmed down to 50 mK. Specific heat, μSR, and NMR measurements all find a majority of dynamic spins and a minority of quasi-static spins mixed in $NaYbSe_2$, which is further supported by thermal conductivity measurements. The ground state of $NaYbSe_2$ can be regarded as a mixed state with both QSL and fluctuating short-range ferrimagnetic droplets, providing a platform to study how disorder influences the QSL state.

MATERIALS AND METHODS

Sample preparation

High-quality $NaYbSe_2$ single crystals were grown by a modified flux method following Schleid and Lissner.[62] Analytically pure Yb powder, Se powder, and NaCl as flux in a molar ratio of 2:3:90 were sealed in a quartz tube and heated to 950°C for 7 days, followed by a maintaining at 950°C for 7 days. The mixture was slowly cooled down to 600°C at a rate of 50°C per day. In the end, reddish-black platelets with largest size of 7–8 mm, as shown in the inset of Figure S1, were separated by dipping in water. The large natural surface was determined to be the (001) plane by X-ray diffraction, as illustrated in Figure S1 and no impurity phases were observed, indicating a relatively high crystallization quality.

Magnetic measurements

The magnetic susceptibility measurements were performed in commercial SQUID and the specific heat was measured in the physical property measurement system (PPMS, Quantum Design) by the relaxation method.

μSR measurements

In a μSR experiment, a beam of nearly 100% spin polarized muon is implanted into the sample. Muon spin precesses and relaxes because of an inhomogeneous local magnetic field. One can measure the time spectra of muon spin polarization, and the relaxation process can reveal the distribution of local field.[28,51,52] Besides, muon is extremely sensitive to small field, which is a powerful technique to check the essence of magnetic order.[53] ZF and LF μSR measurements were performed down to 88 mK on MuSR spectrometer at ISIS, Rutherford Appleton Laboratory, Chilton, UK. Single crystals of $NaYbSe_2$ are aligned so that the c axis is normal to the sample's planar surface and parallel to the initial muon spin polarization and mounted onto a silver holder covering a circle area of 1 inch in diameter and 3 mm in thickness. μSR data were analyzed using the MANTID PROJECT and MUSRFIT software packages.[63] Subtracting the constant background signal due to silver sample holder, ZF muon spin polarization spectra $P(t)$ can be described by the formula $P(t)=fG_{\text{KT}}(\sigma,t)+(1-f)\exp(-\lambda t)$, where $G_{\text{KT}}(\sigma,t)=\frac{1}{3}+\frac{2}{3}(1-\sigma^2t^2)\exp(-\frac{1}{2}\sigma^2t^2)$ is the KT function.[50]

NMR measurements

The ^{23}Na NMR measurements are taken on one piece of $NaYbSe_2$ single crystal with the mass of 2.6 mg. Because the nuclear gyromagnetic ratios for ^{23}Na ($\gamma_{\text{Na}}=11.2625$ MHz/T) is very close to ^{63}Cu ($\gamma_{\text{Cu}}=11.285$ MHz/T), we chose the Ag wire to wind NMR coil. To define the exact external magnetic field, we fill a small piece of Al foil into the coil. The NMR spectra are obtained by the fast Fourier transformation sum of the standard spin-echo signals. The linewidth is extracted from Gaussian fitting. Especially when fitting the spectra of dynamic part between 0.25 K and 1.5 K, we fixed the linewidth of the central line and the satellite line to be the same. The nuclear spin-lattice relaxation rate $1/T_1$ is measured by saturation method below 1.5 K and inverse method for higher temperature. The recovery curve of the nuclear magnetization $M(t)$ is fitted with the function $1-\frac{M(t)}{M(\infty)}=I_0\left\{0.1\exp\left[-\left(\frac{t}{T_1}\right)^{\beta}\right]+0.9\exp\left[-\left(\frac{6t}{T_1}\right)^{\beta}\right]\right\}$. The error bars are determined by the least squares method.

Thermal conductivity measurements

The single crystal selected for the thermal conductivity measurements was a rectangular shape of dimensions 5.38 × 1.30 mm^2 in the ab plane, with a thickness of 0.04 mm along the c axis. The thermal conductivity was measured in a dilution refrigerator, using a standard four-wire steady-state method with two RuO_2 chip thermometers, calibrated *in situ* against a reference RuO_2 thermometer. Magnetic fields were applied along the c axis for specific heat and thermal conductivity measurements and perpendicular to the heat current in the thermal conductivity measurements.

Residual entropy

Assuming each ferrimagnetic droplet carries m spin-1/2 ($J_{\text{eff}}=1/2$ local moment) and the fractional volume of the ferrimagnetic droplets is r, then the effective spin of each droplet is $\overline{S}=\frac{m}{3}\times\frac{1}{2}$, which gives rise to the upper bound of the residual entropy $R\ln(1+2\overline{S})=R\ln(1+m/3)$. Thus, the ratio between the residual entropy and the total magnetic entropy at high temperatures has an upper bound of $\frac{r\ln(1+m/3)}{m\ln2}$.

REFERENCES

1. Anderson, P.W. (1973). Resonating valence bonds: a new kind of insulator? Mater. Res. Bull. ***8***, 153–160.
2. Balents, L. (2010). Spin liquids in frustrated magnets. Nature ***464***, 199–208.
3. Savary, L., and Balents, L. (2017). Quantum spin liquids: a review. Rep. Prog. Phys. ***80***, 016502.
4. Zhou, Y., Kanoda, K., and Ng, T.-K. (2017). Quantum spin liquid states. Rev. Mod. Phys. ***89***, 025003.
5. Takagi, H., Takayama, T., Jackeli, G., et al. (2019). Concept and realization of Kitaev quantum spin liquids. Nat. Rev. Phys. ***1***, 264–280.
6. Broholm, C., Cava, R.J., Kivelson, S.A., et al. (2020). Quantum spin liquids. Science ***367***, eaay0668.
7. Anderson, P.W. (1987). The resonating valence bond State in La_2CuO_4 and superconductivity. Science ***235***, 1196–1198.
8. Kitaev, A. (2006). Anyons in an exactly solved model and beyond. Ann. Phys. ***321***, 2–111.
9. Shimizu, Y., Miyagawa, K., Kanoda, K., et al. (2003). Spin liquid state in an organic Mott insulator with a triangular lattice. Phys. Rev. Lett. ***91***, 107001.
10. Yamashita, S., Nakazawa, Y., Oguni, M., et al. (2008). Thermodynamic properties of a spin-1/2 spin-liquid state in a κ-type organic salt. Nat. Phys. ***4***, 459–462.
11. Yamashita, M., Nakata, N., Kasahara, Y., et al. (2009). Thermal-transport measurements in a quantum spin-liquid state of the frustrated triangular magnet κ-$(BEDT\text{-}TTF)_2Cu_2(CN)_3$. Nat. Phys. ***5***, 44–47.
12. Itou, T., Oyamada, A., Maegawa, S., et al. (2008). Quantum spin liquid in the spin-1/2 triangular antiferromagnetic $EtMe_3Sb[Pd(dmit)_2]_2$. Phys. Rev. B ***77***, 104413.
13. Yamashita, M., Nakata, N., Senshu, Y., et al. (2010). Highly mobile gapless excitations in a two-dimensional candidate quantum spin liquid. Science ***328***, 1246–1248.

14. Yamashita, S., Yamamoto, T., Nakazawa, Y., et al. (2011). Gapless spin liquid of an organic triangular compound evidenced by thermodynamic measurements. Nat. Commun. **2**, 275.
15. Shores, M.P., Nytko, E.A., Bartlett, B.M., and Nocera, D.G. (2005). A structurally perfect S = 1/2 kagome antiferromagnet. J. Am. Chem. Soc. **127**, 13462–13463.
16. Helton, J.S., Matan, K., Shores, M.P., et al. (2007). Spin dynamics of the spin-1/2 kagome lattice antiferromagnet $ZnCu_3(OH)_6Cl_2$. Phys. Rev. Lett. **98**, 107204.
17. Han, T.-H., Norman, M.R., Wen, J.-J., et al. (2016). Correlated impurities and intrinsic spin-liquid physics in the kagome material herbertsmithite. Phys. Rev. B **94**, 060409.
18. Fu, M., Imai, T., Han, T.-H., and Lee, Y.S. (2015). Evidence for a gapped spin-liquid ground state in a kagome Heisenberg antiferromagnet. Science **350**, 655–658.
19. Mendels, P., Bert, F., de Vries, M.A., et al. (2007). Quantum magnetism in the paratacamite family: towards an ideal kagome lattice. Phys. Rev. Lett. **98**, 077204.
20. Banerjee, A., Bridges, C.A., Yan, J.-Q., et al. (2016). Proximate Kitaev quantum spin liquid behaviour in a honeycomb magnet. Nat. Mater. **15**, 733–740.
21. Banerjee, A., Yan, J., Knolle, J., et al. (2017). Neutron scattering in the proximate quantum spin liquid α-$RuCl_3$. Science **356**, 1055–1059.
22. Kasahara, Y., Sugii, K., Ohnishi, T., et al. (2018). Majorana quantization and half-integer thermal quantum Hall effect in a Kitaev spin liquid. Nature **559**, 227–231.
23. Lang, F., Baker, P.J., Haghighirad, A.A., et al. (2016). Unconventional magnetism on a honeycomb lattice in α-$RuCl_3$ studied by muon spin rotation. Phys. Rev. B **94**, 020407.
24. Kitagawa, K., Takayama, T., Matsumoto, Y., et al. (2018). A spin-orbital-entangled quantum liquid on a honeycomb lattice. Nature **554**, 341–345.
25. Li, Y., Liao, H., Zhang, Z., et al. (2015). Gapless quantum spin liquid ground state in the two-dimensional spin-1/2 triangular antiferromagnet $YbMgGaO_4$. Sci. Rep. **5**, 16419.
26. Paddison, J.A., Daum, M., Dun, Z., et al. (2017). Continuous excitations of the triangular-lattice quantum spin liquid $YbMgGaO_4$. Nat. Phys. **13**, 117–122.
27. Shen, Y., Li, Y.-D., Wo, H., et al. (2016). Evidence for a spinon Fermi surface in a triangular-lattice quantum-spin-liquid candidate. Nature **540**, 559–562.
28. Li, Y., Adroja, D., Biswas, P.K., et al. (2016). Muon spin relaxation evidence for the $U(1)$ quantum spin-liquid ground state in the triangular antiferromagnet $YbMgGaO_4$. Phys. Rev. Lett. **117**, 097201.
29. Ding, Z., Zhu, Z., Zhang, J., et al. (2020). Persistent spin dynamics and absence of spin freezing in the $H - T$ phase diagram of the two-dimensional triangular antiferromagnet $YbMgGaO_4$. Phys. Rev. B **102**, 014428.
30. Xu, Y., Zhang, J., Li, Y.S., et al. (2016). Absence of magnetic thermal conductivity in the quantum spin-liquid candidate $YbMgGaO_4$. Phys. Rev. Lett. **117**, 267202.
31. Ma, Z., Wang, J., Dong, Z.-Y., et al. (2018). Spin-glass ground state in a triangular-lattice compound $YbZnGaO_4$. Phys. Rev. Lett. **120**, 087201.
32. Zhu, Z., Maksimov, P.A., White, S.R., et al. (2017). Disorder-induced mimicry of a spin liquid in $YbMgGaO_4$. Phys. Rev. Lett. **119**, 157201.
33. Parker, E., and Balents, L. (2018). Finite-temperature behavior of a classical spin-orbit-coupled model for $YbMgGaO_4$ with and without bond disorder. Phys. Rev. B **97**, 184413.
34. Kimchi, I., Nahum, A., and Senthil, T. (2018). Valence bonds in random quantum magnets: theory and application to $YbMgGaO_4$. Phys. Rev. X **8**, 031028.
35. Kimchi, I., Sheckelton, J.P., McQueen, T.M., et al. (2018). Scaling and data collapse from local moments in frustrated disordered quantum spin systems. Nat. Commun. **9**, 4367.
36. Liu, W., Zhang, Z., Ji, J., et al. (2018). Rare-earth chalcogenides: a large family of triangular lattice spin liquid candidates. Chin. Phys. Lett. **35**, 117501.
37. Baenitz, M., Schlender, P., Sichelschmidt, J., et al. (2018). $NaYbS_2$: a planar spin-1/2 triangular-lattice magnet and putative spin liquid. Phys. Rev. B **98**, 220409.
38. Dai, P.-L., Zhang, G., Xie, Y., et al. (2021). Spinon Fermi surface spin liquid in a triangular lattice antiferromagnet $NaYbSe_2$. Phys. Rev. X **11**, 021044.
39. Bordelon, M.M., Kenney, E., Liu, C., et al. (2019). Field-tunable quantum disordered ground state in the triangular-lattice antiferromagnet $NaYbO_2$. Nat. Phys. **15**, 1058–1064.
40. Ding, L., Manuel, P., Bachus, S., et al. (2019). Gapless spin-liquid state in the structurally disorder-free triangular antiferromagnet $NaYbO_2$. Phys. Rev. B **100**, 144432.
41. Sarkar, R., Schlender, P., Grinenko, V., et al. (2019). Quantum spin liquid ground state in the disorder free triangular lattice $NaYbS_2$. Phys. Rev. B **100**, 241116.
42. Ranjith, K.M., Dmytriieva, D., Khim, S., et al. (2019). Field-induced instability of the quantum spin liquid ground state in the J_{eff} = 1/2 triangular-lattice compound $NaYbO_2$. Phys. Rev. B **99**, 180401.
43. Bordelon, M.M., Liu, C., Posthuma, L., et al. (2020). Spin excitations in the frustrated triangular lattice antiferromagnet $NaYbO_2$. Phys. Rev. B **101**, 224427.
44. Ranjith, K.M., Luther, S., Reimann, T., et al. (2019). Anisotropic field-induced ordering in the triangular-lattice quantum spin liquid $NaYbSe_2$. Phys. Rev. B **100**, 224417.
45. Xing, J., Sanjeewa, L.D., Kim, J., et al. (2019). Field-induced magnetic transition and spin fluctuations in the quantum spin-liquid candidate $CsYbSe_2$. Phys. Rev. B **100**, 220407.
46. Wu, J., Li, J., Zhang, Z., et al. (2022). Magnetic field effects on the quantum spin liquid behaviors of $NaYbS_2$. Quantum Front. **1**, 13.
47. Jia, Y.-T., Gong, C.-S., Liu, Y.-X., et al. (2020). Mott transition and superconductivity in quantum spin liquid candidate $NaYbSe_2$. Chin. Phys. Lett. **37**, 097404.
48. Zhang, Z., Yin, Y., Ma, X., et al. (2020). Pressure induced metallization and possible unconventional superconductivity in spin liquid $NaYbSe_2$. Preprint at arXiv. https://doi.org/10.48550/arXiv.2003.11479.
49. Zhang, Z., Ma, X., Li, J., et al. (2021). Crystalline electric-field excitations in quantum spin liquids candidate $NaYbSe_2$. Phys. Rev. B **103**, 035144.
50. Hayano, R.S., Uemura, Y.J., Imazato, J., et al. (1979). Zero- and low-field spin relaxation studied by positive muons. Phys. Rev. B **20**, 850–859.
51. Luke, G.M., Fudamoto, Y., Kojima, K.M., et al. (1998). Time-reversal symmetry-breaking superconductivity in Sr_2RuO_4. Nature **394**, 558–561.
52. Uemura, Y.J., Yamazaki, T., Harshman, D.R., et al. (1985). Muon-spin relaxation in AuFe and CuMn spin glasses. Phys. Rev. B **31**, 546–563.
53. Choi, S.K., Coldea, R., Kolmogorov, A.N., et al. (2012). Spin waves and revised crystal structure of honeycomb iridate Na_2IrO_3. Phys. Rev. Lett. **108**, 127204.
54. Zhang, Z., Li, J., Xie, M., et al. (2022). Low-energy spin dynamics of the quantum spin liquid candidate $NaYbSe_2$. Phys. Rev. B **106**, 085115.
55. Yoshida, M., Takigawa, M., Yoshida, H., et al. (2011). Heterogeneous spin state in the field-induced phase of volborthite as seen via ^{51}V nuclear magnetic resonance. Phys. Rev. B **84**, 020410.
56. Bert, F., Bono, D., Mendels, P., et al. (2005). Ground state of the kagome-like S = 1/2 antiferromagnet volborthite $Cu_3V_2O_7(OH)_2 \cdot 2H_2O$. Phys. Rev. Lett. **95**, 087203.
57. Sutherland, M., Hawthorn, D.G., Hill, R.W., et al. (2003). Thermal conductivity across the phase diagram of cuprates: low-energy quasiparticles and doping dependence of the superconducting gap. Phys. Rev. B **67**, 174520.
58. Li, S.Y., Bonnemaison, J.-B., Payeur, A., et al. (2008). Low-temperature phonon thermal conductivity of single-crystalline Nd_2CuO_4: Effects of sample size and surface roughness. Phys. Rev. B **77**, 134501.
59. Nave, C.P., and Lee, P.A. (2007). Transport properties of a spinon Fermi surface coupled to a $U(1)$ gauge field. Phys. Rev. B **76**, 235124.
60. Lee, S.-S., and Lee, P.A. (2005). $U(1)$ gauge theory of the Hubbard model: spin liquid states and possible application to κ-$(BEDT\text{-}TTF)_2Cu_2(CN)_3$. Phys. Rev. Lett. **95**, 036403.
61. Werman, Y., Chatterjee, S., Morampudi, S.C., et al. (2018). Signatures of fractionalization in spin liquids from interlayer thermal transport. Phys. Rev. X **8**, 031064.
62. Schleid, T., and Lissner, F. (1993). Single crystals of $NaMS_2$ (M: Ho-Lu) from reactions of the lanthanoids with sulfur in the presence of NaCl. Eur. J. Solid State Inorg. Chem. **30**, 829.
63. Suter, A., and Wojek, B. (2012). Musrfit: a free platform-independent framework for μSR data analysis. Phys. Procedia **30**, 69–73.

ACKNOWLEDGMENTS

We thank Y. Xu for helpful discussions. This research was funded by the National Key R&D Program of China (Grant No. 2022YFA1402203), the National Natural Science Foundation of China of China (Grant No. 12034004, No. 11774061, and No. 11774306), the Shanghai Municipal Science and Technology (Major Project Grant No. 2019SHZDZX01, No. 20ZR1405300, and No. 23ZR1404500), the Strategic Priority Research Program of Chinese Academy of Sciences (No. XDB28000000), and the Innovation program for Quantum Science and Technology (Grant No. 2021ZD0302500).

AUTHOR CONTRIBUTIONS

L.S. and S.L. planned the project. B.P. synthesized the sample, and characterized the sample with C.J. Z.Z., Y.Yang, and C.C. carried out the μSR experiments with experimental assistance from A.D.H. L.N. carried out the NMR experiments. B.P., J.N., Y.H., E.C., and Y.Yu performed the thermal conductivity measurements. L.S., S.L., T.W., Z.Z., B.P., L.N., and J.N. analyzed the data. Y.Z. and J.M. provided the theoretical explanation. L.S., S.L., T.W., Y.Z., X.C., Z.Z., B.P., and L.N. wrote the paper.

DECLARATION OF INTERESTS

The authors declare no competing interests.

DATA AVAILABILITY

All data needed to evaluate the conclusions in the paper are present in the main text or the supplemental information.

SUPPLEMENTAL INFORMATION

It can be found online at https://doi.org/10.1016/j.xinn.2023.100459.

LEAD CONTACT WEBSITE

http://www.physics.fudan.edu.cn/tps/people/leishu/grouphomepage.html.